Morphology Formation in Polypropylene Impact Copolymers Under Static Melt Conditions: A Simulation Study

Klaas Remerie,[1] Jan Groenewold[2]

[1]*Sabic T&I, STC Geleen, P.O. Box 319, 6160 AH Geleen, The Netherlands*
[2]*Department of Chemistry, Utrecht University, 3584 CH Utrecht, The Netherlands*

Received 6 January 2011; accepted 11 August 2011
DOI 10.1002/app.35463
Published online 17 December 2011 in Wiley Online Library (wileyonlinelibrary.com).

ABSTRACT: In this article, the equilibrium morphology of a typical polypropylene (PP) impact copolymer (ICP) system is investigated by numerical self-consistent field simulations. The ICP was fractionated using temperature rising elution fractionation (TREF) to obtain the data necessary to define the simulation parameters. The results demonstrated the formation of a stratified droplet structure, in which ethylene content decreases from the center of the droplet toward the PP interface. This structure is shown to be in accordance with observations from transmission electron microscopy, scanning electron microscopy, and atomic force microscopy. The components are confined to a narrow layer whose position is primarily determined by its ethylene content. Leakage into a neighboring layer occurs to a degree that is determined by the component molecular weight and the difference in ethylene content between the layers. Simulations for a range of droplet sizes enable calculation of the interfacial tension. A typical drawback of TREF involves the inability to fractionate the amorphous part, leading to a large difference in ethylene content between the matrix and its neighboring layers. Although this effect is shown not to have a significant influence on the stratified structure, it is shown to have a significant influence on the derived interfacial tension. © 2011 Wiley Periodicals, Inc. J Appl Polym Sci 125: 212–223, 2012

Key words: polymer science; simulation; polypropylene

INTRODUCTION

Polypropylene (PP) is one of the most important commercial polymers available[1] because of its favorable price/performance relation in a wide range of applications ranging from highly demanding automotive applications to textiles and household products. Homopolymers are especially valued for their high stiffness. However, structural applications, for example, automotive bumpers, require polymers exhibiting higher impact resistance, particularly at low temperatures. Purely isotactic PP, characterized by a relatively high glass transition temperature ($T_g \approx 0$°C), is therefore too brittle for such end-use applications. Improvement of impact strength may be achieved by the incorporation of discrete rubbery domains in the brittle polymer matrix.

Although blends of PP with several types of elastomer have been investigated [including butyl rubber, styrene–butadiene–styrene copolymer, ethylene–propylene rubber (EPR), and ethylene–propylene–diene copolymer], in-reactor blends of (typically) PP homopolymer (PPH) and EP copolymer, often called impact copolymers (ICPs) or heterophasic copolymers, largely dominate the commercial arena.[2]

A typical ICP is prepared by starting the polymerization in a first reactor system in which typically a PPH is produced. This material, still containing active catalyst, is then transferred to a second reactor system in which the EP copolymer is produced. Typically, ICP polymerization is catalyzed by a (heterogeneous) Ziegler-Natta catalyst.[3]

As shown by Debling and Ray[4] and Kakugo et al.,[5,6] a nascent PP powder particle consists of several mesoparticles, or polymer globules, characterized by a diameter of the order of 1 μm. Each mesoparticle consists of primary polymer microparticles formed around a catalyst active center. The second-stage EPR, being formed at these still active catalyst centers, finds its way into the pores and cracks in the homopolymeric material produced in the first stage, resulting in a finely dispersed system, as observed in Figure 1 (left image).

Because of their thermodynamic incompatibility,[7] demixing of the PP and EPR phases takes place on melting toward a disperse morphology characterized by a EPR particle size distribution typically in the range of 0.5–2 μm, as shown in Figure 1 (right image).

Correspondence to: K. Remerie (klaas.remerie@sabic-europe.com).

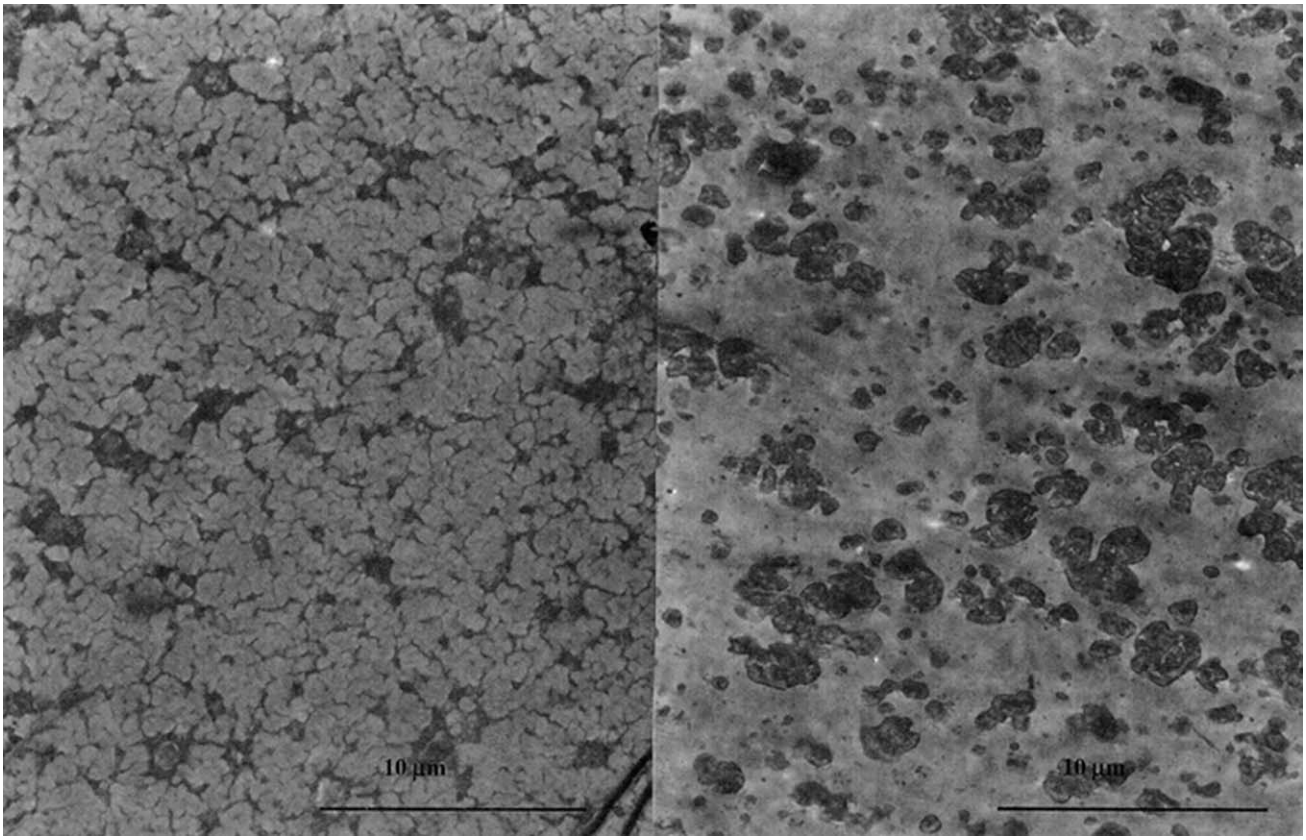

Figure 1 Morphology of PP ICP as characterized by TEM (for composition data, see Table I). At the left the nascent powder, at the right the disperse morphology after melt extrusion.

The heterogeneous nature of the ZN catalyst is generally assumed to be responsible for a rather broad molar mass distribution (MMD) and tacticity distribution by means of a distribution of several types of (Flory-type) active sites.[8,9] This distribution of sites also implies a rather broad chemical composition distribution (CCD), which indeed is experimentally observed by temperature rising elution fractionation (TREF) and crystallization fractionation (CRYSTAF).[10–14] This structural heterogeneity is generally assumed to compatibilize the interface between the high ethylene-containing part of the elastomer phase and the PP matrix, resulting in a typical disperse phase morphology as depicted above, thereby leading to an improved balance of mechanical properties when compared with extruder blends.[11,12,14–17]

Considering this strong dependence of the mechanical properties of such biphasic systems on not only structural but also on morphological characteristics, it is clear that a thorough understanding of the way structural parameters control phase evolution during extrusion from powder to pellet and phase stability during processing is of paramount importance for grade development.

In qualitative terms, the influence of MM, MMD, and crystallinity of the PP matrix, as well as the composition of the blends and the molecular structure of the rubbery phase, e.g., ethylene content, CCD, MM, and MMD, on phase morphology have been reported.[16–19] The size and size distribution of the disperse phase in such multiphase systems are shown to depend primarily on the viscosity of both phases and on their compatibility[11,12,19–22] as well as on the processing conditions applied.[23,24] However, up to now, the predictive value of the various reported model-based approaches regarding morphology has been rather unsatisfactory.

The Flory-Huggins approach is generally a valid approach to predict phase diagrams for apolar systems, as their phase behavior is primarily governed by dispersion forces. Usually a two-component version of the Flory-Huggins theory is applied to describe the phase behavior of ICP blends.[7] This approach constitutes a strong oversimplification in view of the polydispersity described above. However, lack of reliable data about molecular composition and the additional theoretical complexity to treat such blends have prevented the use of a more realistic thermodynamic modeling of these systems.

In this contribution, we will demonstrate how the use of an advanced modeling and computational toolbox, as provided by the CULGI Library, more specifically, self-consistent field (SCF) simulations enable to cope with the dramatic increase of complexity resulting from the introduction of polydispersity in the homopolymer as well as in the copolymer phase, together with a broad CCD within the copolymer phase.

TABLE I
Polymer Compositions

Product	MFI (230°C, 2.16 kg) (dg/min)	Rubber content (wt %)	Rubber ethylene content (wt %)
Homopolymer	4.7	–	–
Impact copolymer	1.5	25	60

EXPERIMENTAL

Materials

A typical ICP composition containing 25 wt % rubber and 60 wt % ethylene in the rubber phase was produced on laboratory scale. Additionally, a homopolymer, using polymerization conditions and catalyst recipe identical to that of the ICP homopolymer phase, was separately produced. Some typical data for both polymers are provided in Table I.

Polymer analysis

Fractionation

Fractionation of the materials is carried out by preparative TREF. Both the ICP and the PPH have been fractionated using identical temperature intervals. In a typical preparative TREF analysis of PPH, a polymer solution is prepared at 130°C in xylene and placed into a column prepacked with sand, after which the fractionation procedure is carried out. For the fractionation of ICP, the procedure essentially is identical; however, a prefractionation is carried out at 98°C to separate the high isotactic PPH part from the ethylene-containing polymer. This prefractionation is important to increase the separation efficiency of the various ethylene-containing fractions. The ethylene-containing material is subsequently further fractionated using the defined temperature intervals.

By using the homopolymer fractionation result and the homopolymer content in the ICP, the weight fractions of the ICP rubber fractions, which always contain lower tactic homopolymer fractions, can be corrected for the amount of homopolymer.

Molar mass distribution

The ICP homopolymer matrix and all rubber fractions are analyzed in terms of MMD obtained using size exclusion chromatography equipped with a viscosity detector (SEC-DV). In the SEC chromatogram of most rubber fractions, bimodality is observed; in all cases, a low MW peak is assigned to the lower tactic homopolymer fraction; and a higher MW peak is characteristic for the EP rubber component. The peak value of this last peak is used as input for the simulations.

Ethylene content

The ethylene content of the various rubber fractions is determined by ^{13}C-NMR and corrected for the lower amount of tactic homopolymer present (Table II).

SELF-CONSISTENT FIELD SIMULATIONS

The present theoretical analysis of EPR disperse droplet structure is based on SCF theory. This is a suitable method for polymer blends with weak inhomogeneities, i.e., polymer blends with a small Flory χ parameter. This SCF approach is a generalization of the Flory-Huggins model[25] for polymer blends. Apart from the description of the (thermodynamic) equilibrium structure of a polymer blend system, the SCF approach can also incorporate dynamic aspects in polymers melts.[26,27] In the current study, we will use only the dynamic aspect as a tool to find the thermodynamic equilibrium structure in the droplet. Computer simulations were carried out using the CULGI software package. CULGI[26] builds further on the mean field (or SCF) approach, as developed by Helfand[28] in the early 1970s. Calculations are performed numerically assuming discrete Gaussian chains subject to a self-consistent background potential to evaluate the equilibrium structure. The conformation of polymer chains is computed in the mean field approach as if all chains were subject to an external potential that is consistent with the average concentration of the polymer species.

The basic statistical entity for an SCF approach is the bead. In essence, the bead concept is a coarse graining that considerably reduces computational effort. Each polymer chain may be described as a sequence of beads. A bead, not to be confused with a chemical monomer unit, is an array of chemical monomers representing a segment of a chain, as depicted in Figure 2. In this case, ethylene units (black) and propylene units (white) are combined to produce an average bead, characterized by its gray color (i.e., average ethylene content). In this bead, the average composition of the chain segment is

TABLE II
Composition Data for Rubber Fractions (Corrected for Lower Tactic Homopolymer)

Fraction	Amount (wt %)	Ethylene content (wt %)	M_w (kDa)	M_n (kDa)
1	3.1	98	590	110
2	6.1	96	550	175
3	6.1	85	510	120
4	13.2	83	588	143
5	9.2	78	450	105
6	7.1	69	410	100
7	55.2	37	650	210

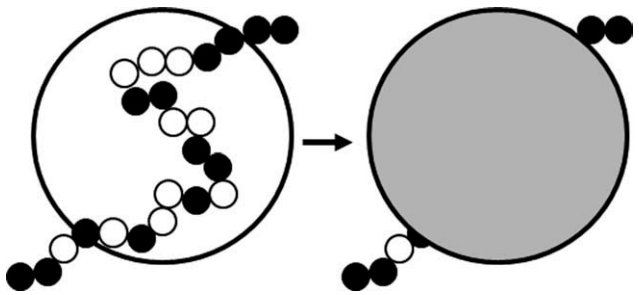

Figure 2 Formation of a bead.

represented by a single effective Flory interaction parameter. Within the SCF approach such a chain segment is also assumed to obey Gaussian statistics. The system thus includes a number of different rubber compositions (as characterized by TREF) with associated bead types, each one exhibiting a different ethylene content.

Although it could be argued that the bead concept introduces a significant oversimplification of a real situation, we have shown that the representation of a polymer chain of $\sim 10^4$ monomers with 1–10 beads provides a realistic description of the real system.[29]

DETERMINATION OF THE SIMULATION PARAMETERS

Parameterization of the enthalpic interactions

To use the SCF approach to determine the equilibrium structure of an EPR droplet in a PP matrix, a proper identification of the model parameters with the actual system parameters should be performed. Various values of the Flory interaction parameter between an ethylene unit and a propylene unit, $\chi_{\text{ethylene/propylene}}$, have been reported. For instance, Kamdar et al.[7] and Lohse et al.[30] reported values of 0.0238 and 0.0169, respectively. Based on these values, a representative $\chi_{\text{ethylene/propylene}}$ of 0.020 was chosen for further analysis.

In a numerical SCF calculation, the χ parameter describing the interaction between two beads will depend on the number of monomers fitted within the beads as well as the ethylene content of the beads. We use the expression derived for the interaction parameter of a copolymer mixture[31,32] to transform the monomer–monomer interaction parameter $\chi_{\text{ethylene/propylene}}$ into a bead–bead interaction parameter χ_{IJ}, as shown in the following equation:

$$\chi_{IJ} = (f_I - f_J)^2 n \chi_{\text{ethylene/propylene}}, \quad (1)$$

Herein, n is the number of monomers within a bead and f_I and f_J represent the ethylene fractions of bead I and J, respectively.

In our simulation, we will use beads containing 200 monomers, which correspond to an interaction energy between a bead of pure ethylene and a bead of pure propylene of 4 kT. Such a bead exhibits a typical diameter of 3.5 nm, which roughly corresponds to the extension of an ethylene–propylene segment of 200 monomers.

The constant ethylene fraction across the chain of each component is a plausible assumption for ZN polymerization under normal conditions. Nonetheless, variation of chemical composition can still occur as a consequence of statistical fluctuations, as the ethylene content is varying, strictly speaking, at least on the monomer scale. In this respect, it should be noted that coarse graining will considerably reduce this variation on the monomer scale. For a bead consisting of 200 monomer units in the present examples, the actual χ parameter typically varies with $\sim$ 7%, which corresponds to enthalpy differences of 0.3 kT when compared with the average of 4 kT.

Finally, the following simulations were performed in a one-dimensional (1D) geometry, i.e., in a box of dimensions $1 \times 1 \times L$, where L is the long dimension of the box. The units consist of bead diameter and the box is subject to reflecting boundary conditions. In a recent paper, we argued the validity of using a 1D approach as compared with the computationally more demanding 3D approach, as long as in the simulation of a real system, proper care is taken to adjust for the shell thickness.[33]

Simulation parameters: MM and CCD

In an ICP, produced by a ZN catalyst system, the structure of matrix and rubber phase may be described by MMD, as well as the three rubber composition parameters: average chemical composition, compositional heterogeneity, and sequence distribution of comonomer units along the chain. Depending on these factors, different kinds of copolymers, from amorphous to partially crystalline, may be obtained.

Chemical composition distribution

In our simulations, we will take the number of rubber components equal to the number of fractions obtained by TREF. Average ethylene content on bead level is taken identical to the average ethylene content of the corresponding fraction. This implies that we treat the copolymer as a statistical copolymer, which is a realistic assumption.

One drawback of TREF however, is that only components with different crystallizability can be separated by fractionation. Depending on the ethylene content of the rubber phase and the catalyst system, 50% or more of the rubber is entirely amorphous, and as a consequence it will be observed as one single component. Although it seems obvious that the broad composition distribution is characteristic of the entire

TABLE III
Simulation Parameters of Rubber Fractions

Fraction	Amount (wt %)	Ethylene content (wt %)	M_w (kDa) High	Medium	Low
1	3.1	98	923	316	69
2	6.1	96	942	323	105
3	6.1	85	883	240	70
4	13.2	83	979	286	86
5	9.2	78	780	210	63
6	7.1	69	639	179	59
7 (*)	55.2	37	1111	383	125
7 (**)	18.4	50	1111	383	125
8 (**)	18.4	37	1111	383	125
9 (**)	18.4	24	1111	383	125

*Unmodified TREF data.
**Interpolated TREF data; for this interpolation, the molecular weight distribution is assumed independent of interpolated ethylene content.

rubber phase, including the amorphous part, till date, no method exists to quantitatively resolve this distribution of the amorphous part. To obtain a qualitative indication of the effect of such a distribution in the amorphous part, in addition to the case in which we treated the TREF fractions as obtained, we also defined an interpolated case. In the interpolated case, the amorphous component was split up in three equal parts where one of the parts in terms of ethylene content is defined in between the lowest "crystalline fraction" and the third at a lower ethylene content such that the average composition of the three fractions complies to the original TREF fraction (Table III). For this interpolation, it was assumed that the MMD is independent of the ethylene content. This is the reason of the repetition of the molar masses in Table III for the interpolated ethylene fractions of 24, 37, and 50%.

Molar mass distribution

The MMDs of the homopolymer fraction and the rubber fractions (corrected for lower isotactic homopolymer) were translated into parameters to be used in the CULGI simulations. The MMD of the ICP homopolymer matrix is characterized by an M_w/M_n of 5.2. For the simulations, it is necessary to divide this broad MMD into several narrower MMDs. As observed in Figure 3, it was arbitrarily chosen, for the current example, to split the MMD into seven components, in such a way that identical weight fractions were obtained. The weight-average molar masses, M_w, of these components are given in Table IV.

Similarly, the MMDs of EPR TREF fraction were divided into three components each (see Table III). The amounts of these components were determined according to the TREF data and thus, together with their ethylene contents, provided a realistic and detailed description of the MMD and CCD of the rubber phase.

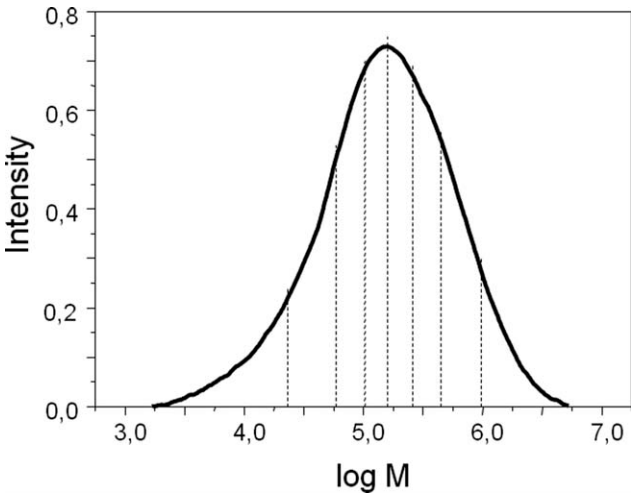

Figure 3 Molar mass distribution of a PP homopolymer and translation into CULGI parameters.

RESULTS ON MORPHOLOGY

Equilibrium morphology using unmodified TREF input

The ICP equilibrium morphology was simulated in 1D using the simulation procedure described above and a parameter set derived from unmodified TREF data as well as interpolated TREF data. The thicknesses of the shells have been corrected to correspond to the real thickness in 3D. In Figure 4, the distribution of the various fractions is shown for the unmodified case. (For simplicity, the effect of molecular weight is not shown and the PP components are also not shown.) In this figure, therefore, an indication of the radial density profiles for each EPR fraction in addition to the local ethylene fraction is given. The center of the box, which is also the center of the disperse droplet, has been chosen as the origin.

Clearly, a stratified morphology has been developed, in which essentially three "shells" have formed: the center one consisting of the highest ethylene contents (98 and 96%); the intermediate one containing the intermediate compositions (85 and 83%); and the

TABLE IV
M_w of the Components Describing the MMD of the ICP Homopolymer Phase

Component	1	2	3	4	5	6	7
M_w (kDa)	972	442	259	160	102	59	23
Log M_w	5.99	5.65	5.41	5.20	5.01	4.77	4.36
Wt. fraction (%)	14.3	14.3	14.3	14.3	14.3	14.3	14.3

The full distribution was separated into seven equal parts each of volume fraction 1/7. The molar mass of each part is then the M_w of that part, which will serve as a single component for the simulation.

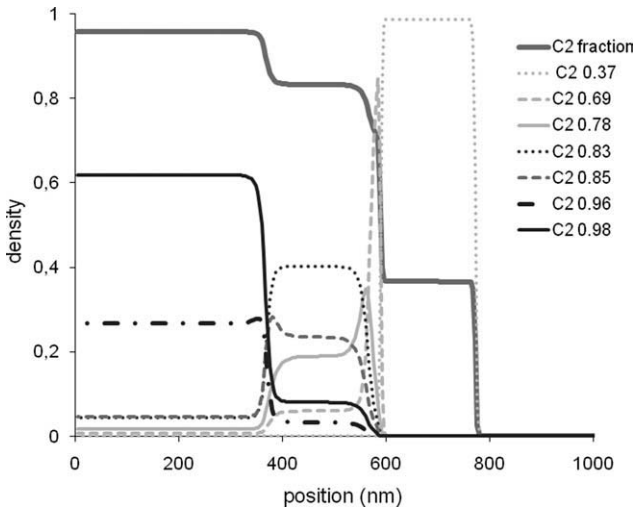

Figure 4 Equilibrium distribution of different ethylene fractions from the unmodified TREF data. The center of the rubber droplet is chosen as the origin.

37% ethylene content material forming the outer layer. The 69% ethylene content material shows a rather special case. Although it shows a considerable solubility in the intermediate layer, most of the material concentrates at the interface of the intermediate and outer layer; however, the amount being too low to form a shell of its own. Despite the onion-like structure, as clearly evidenced by the ethylene profile, partial solubility of material concentrating in one shell in a neighboring shell is evident. This effect is expected to depend on the molecular weight; for lower molecular weights, the entropy term will contribute slightly more to a lowering of free energy at constant enthalpy contribution.

This indeed is shown to be the case when considering the various molecular weights per ethylene content. As an example, we present the distributions for all three molecular weight components for ethylene contents 69 and 37%. Figure 5 shows the three distributions for 69% ethylene content. The profound influence of molecular weight is clear. The lowest molecular weight largely dissolves in the intermediate layer, this is less so for a molecular weight of 179 kDa, whereas the highest molecular weight (639 kDa) is fully confined to the interlayer region.

In contrast, because of the large composition difference with neighboring layers, the shell containing the fractions with 37 wt % ethylene does not leak into neighboring shells at all (Fig. 6). This shell is almost homogeneous, apart from a very slight tendency for the lowest molecular weight to enrich toward both interfaces.

Equilibrium morphology using interpolated TREF input

As clearly shown in Figure 7, the interpolated TREF data essentially lead to a similar stratified equilibrium

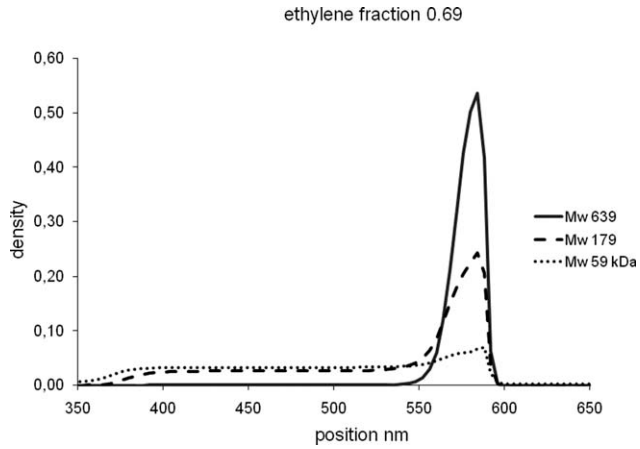

Figure 5 Distributions by M_w component for the unmodified TREF fraction with 69 wt % ethylene.

morphology when compared with the unmodified data; however, the main difference being that the (very large) 37 wt % ethylene shell in the unmodified TREF data is split up in three smaller shells.

Obviously, the overall ethylene profile shows a more smooth behavior in the low ethylene content area, which might influence the interfacial tension (see below). Although the step from ethylene content of 69 to 50 wt % still is too large to permit substantial leakage between the two compositions (Fig. 8), the smaller difference of 13 wt % between the three "interpolated" compositions allows significant leakage of lower molecular weight components as evidenced by the 37 wt % ethylene profile (Fig. 9).

RESULTS ON INTERFACIAL TENSION

Although for interfaces in simple two-phase systems the interfacial tension is a clearly defined and useful quantity, it is less obvious how to define interfacial tension for multicomponent mixtures that have very

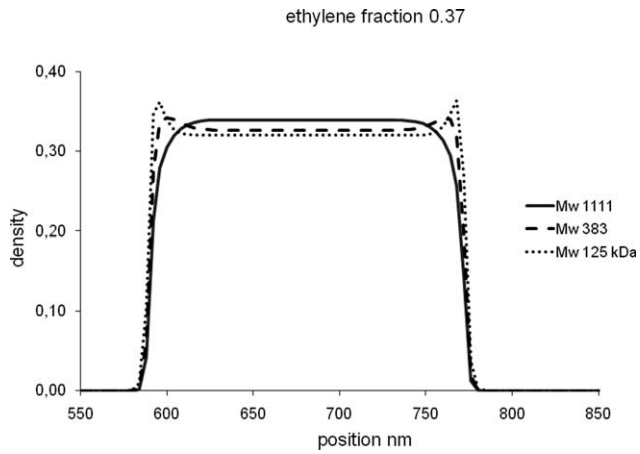

Figure 6 Distributions by M_w component for the unmodified TREF fraction with 37 wt % ethylene.

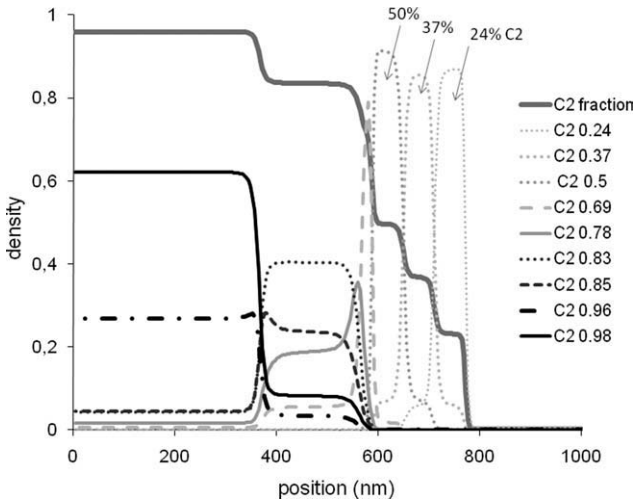

Figure 7 Equilibrium distribution of different ethylene fractions of the interpolated TREF data. The center of the rubber droplet is chosen as the origin.

broad interfaces. We have designed a procedure that permits the calculation of interfacial tension in systems featuring broad interfaces.[33] In short, the procedure involves successive simulation of a system with increasing droplet size keeping the average density of each component exactly the same. A plot of the equilibrium free energy per grid point against the inverse system size allows to derive the interfacial tension from the (local) slope. In the same study, we have shown that the insertion of a broad composition distribution of A–B copolymers at the interface between polymers A and B reduces interfacial tension; however, so far, not to the extent which might be expected. This can be explained when it is considered that the distribution of A–B copolymers forms a phase of its own. Essentially, this means that instead of a single interface which is compatibilized by a continuous distribution, two interfaces are formed, with both a characteristic interfacial tension, adding up to a value of (in our specific

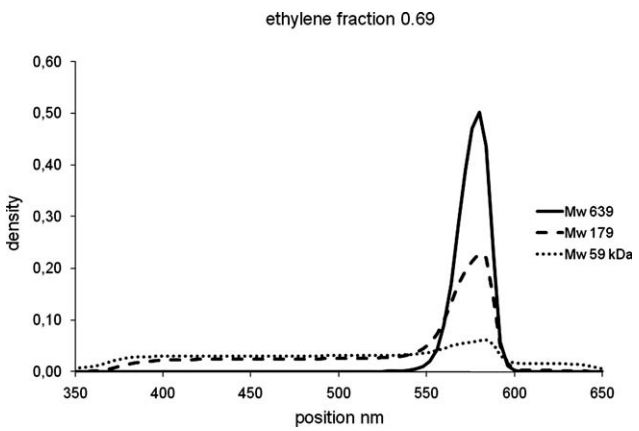

Figure 8 Simulation with interpolated TREF data: distributions by M_w component for the fraction with 69 wt % of ethylene.

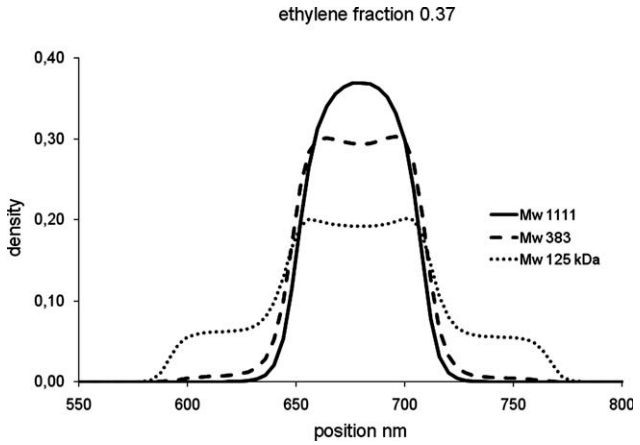

Figure 9 Simulation with interpolated TREF data: distributions by M_w component for the fraction with 37 wt % of ethylene.

example) of about 40% of the value for the uncompatibilized interface. For the present example of a "real" ICP, this raises the important question that how critical the exact distribution of the amorphous material is for the magnitude of the interfacial tension.

In the same publication,[33] we have also focused on the influence of the average composition in a chain on the interfacial tension. The motivation for doing so was to find out what the impact of such broad distribution can be. By considering the energetics of each chain it will be argued below that the positioning of the chains within a drop will be dominated by the average ethylene content and that the intrachain compositional fluctuations are expected to be a less important factor. In case of the interfacial tension, however, it is known that compositional fluctuations can give rise to a (usually modest) lowering of the interfacial tension in the case of a two-phase system in which average compositions of the copolymer phases are comparable with "pure" homopolymer phases.[34] To see the effect of intrachain fluctuations, two separate cases were considered: (1) the case in which only interchain compositional fluctuations were taken into account and (2) the case in which both intrachain and interchain compositional fluctuations were taken into account.

Next to the effect of intrachain compositional fluctuations, we also investigate the effect of interchain composition on interfacial tension by comparing the composition as analyzed by TREF with the already discussed interpolated case.

Only interchain variation in composition

As the TREF procedure applied does not permit to resolve the composition distribution of the amorphous material, the difference in interfacial tension as computed for the unmodified and interpolated TREF data is of crucial importance when assessing

the relevance of TREF data for judging compatibilization effects of different rubber structures. Therefore, we applied the same procedure to determine interfacial tension for the unmodified and interpolated TREF data.

For reference, the uncompatabilized interfacial tension should also be given. To keep simulations tractable, we chose to work with a simulation χ value of 4.0 for a bead of pure ethylene interacting with a pure propylene bead. On average, these beads consist of 200 chemical monomers. To simulate a blend of pure homopolymers with such a high value of χ is way beyond the validity of SCF theory. However, we have not been simulating in a pure blend, but rather in a multicomponent system with more modest steps in effective χ between the neighboring phases. Within the simulations performed in this study, the maximum jump in ethylene content between two neighboring shells or phases is 37%, which is the jump between the PPH and the first shell of the EPR droplet. For our choice of interaction parameters, this jump exhibits an effective χ parameter of 0.45. The results for interfacial tension of the ICP are compared with a two component blend (PP-PE) that has a simulation χ parameter of 0.45. The molecular weights are chosen such that the average molecular weight of the polyethylene (PE) phase corresponds to the average molecular weight of the EPR phase and the molecular weight of the reference PP phase is given by the average molecular weight of the actual PPH matrix. Note that it is well known that numerical SCF calculations where the effective χ parameter between neighboring phases exceeds 0.5 give erroneous results. Furthermore, it must be recognized that course graining (choosing a higher maximum χ parameter so that a bead consists of more monomers) also introduces a small error because the effect of chain ends is overestimated. In Figure 10, the reference case of a pure PP/PE blend of 200 kDa PE chains and 100 kDa PP chains is shown. Note that this simulation was performed with less chemical monomers per bead due to the lower χ value (0.5 compared to 4). To compare the simulations with different χ (keeping $M\chi$ equal, with M the number of beads), an appropriate scaling with the square root of χ must be applied. In Figure 10, this scaling has been applied on the y-axis.

To fix the value on the surface tension scale, a determination of the interfacial tension at $\chi = 0.125$ has been performed with $M\chi = 25$. The simulation result is $\gamma = 0.155$, which should be compared to the asymptotically exact expression by Helfand and Tagami[35]:

$$\gamma = kT\frac{b}{v}\left(\frac{\chi}{6}\right)^{1/2}, \qquad (2)$$

With kT the thermal energy, b the length of a Kuhn segment, and v the volume of a Kuhn segment,

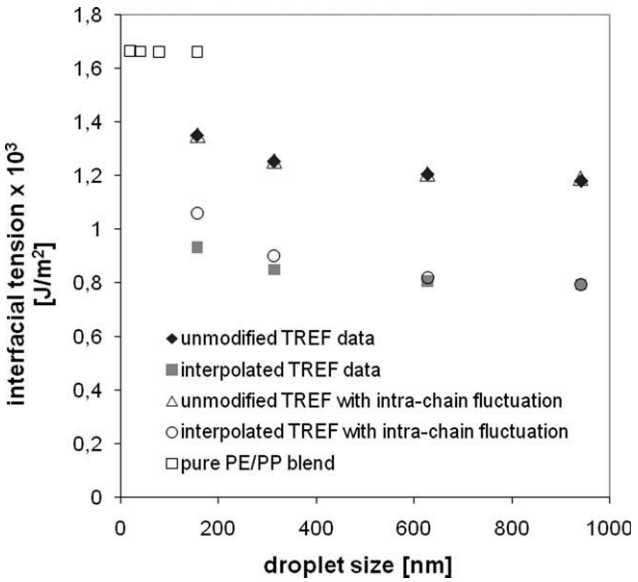

Figure 10 Interfacial tension as a function of droplet size for unmodified and interpolated TREF data. In addition, both these cases are evaluated with and without intrachain compositional fluctuations. The reference interfacial tension of a pure PE/PP blend is also given.

which in the simulation are all set to unity. With the simulation values, the Helfand–Tagami value is found to be $\gamma = 0.144$ for $\chi = 0.125$, a value sufficiently close to the one obtained by simulation.

At the same time, the expected interfacial tension can be derived for the PE/PPH blend through the same expression [eq. (2)] using experimental parameters. The result is $\gamma_{PE/PP} = 1.66 \times 10^{-3}$ J/m^2. (Here, the value for $\chi = 0.02$, the Kuhn segment length and Kuhn segment volume are the geometric mean of the values for pure PE and PP taken from Ref. 36.) Combining this reference value with the square root dependence on χ allows us to fix the absolute interfacial tension scale of Figure 10. Also for the horizontal axis in Figure 10 a similar scaling has been applied in order to compare the different simulations.

The preceding paragraph reflects that comparing simulations performed at different levels of coarse graining (by choosing different χ parameters while keeping $M\chi$ equal) needs some care. This complication does not arise as long as the simulations are being compared using the same level of course graining. Note that apart from the reference system of pure PE and PP, the simulations were performed using the same value level of coarse graining, i.e., with $\chi = 4$, which corresponds to a grid size of 3.5 nm per grid point.

Both intrachain and interchain compositional variation

To assess the possible relevance of intrachain randomness or compositional variation, let us consider

the following numerical example: on the scale of a real polymer of about 400 kDa, the enthalpic difference between one half of the chain and the other half will typically be in the order of 1.4 kT (based on purely random fluctuations in chemical composition). This implies that a chain may orient itself in a density gradient emerging in a drop. Another consequence of the statistical fluctuation is the increased compatibilizing property compared with a fully homogeneous composition. In one case, this effect is neglected by imposing a constant ethylene fraction, f_n, along the chain. This assumption emphasizes the effect of a different ethylene fraction for each species, which is considered much more important than variations of χ within a chain. Indeed, the enthalpy difference between a 400-kDa chain with 40% ethylene compared with 50% is about 20 kT, which is much more than the 2 kT difference between one end and the other. Considering these differences we do not expect much impact on the positions of the chains themselves. However, stretching and local compatibilization effects can have influence. To establish this influence, a simulation that explicitly invokes this randomness will be performed.

To assess the effect of intrachain randomness, the same MMD and CCD is considered but with realistic compositional fluctuations within a chain. To parameterize the compositional fluctuations within a bead, we will introduce two types of beads (say "*A*" and "*a*") for each average ethylene fraction. Of these beads, random copolymers of the prescribed length will be formed (e.g., *AaaAAaAaAaaa*). The "*A*" bead will have a slightly larger ethylene fraction than the "*a*" bead such that the average equals the prescribed ethylene fraction. In addition, the ethylene fraction of *A* and *a* will be chosen such that the fluctuation in each bead reflects the expected fluctuation in ethylene content of each bead. Based on a purely random distribution of a sequence of *n* beads with equal probability of *a* and *A* beads, one finds that the compositional fluctuations can be represented as follows:

$$f_A = f + \Delta f \; ; \; f_a = f - \Delta f,$$

$$\Delta f = \sqrt{f - f^2} \; \frac{1}{\sqrt{n}}, \tag{3}$$

Here, the fluctuation in ethylene fraction Δf is related to the average ethylene fraction f. The expressions from eq. (3) for the effective local ethylene fraction can now be used to calculate the effective bead–bead interaction parameters with eq. (1).

In Figure 10, we visualize the relation between droplet size and interfacial tension for all cases described so far. The "equilibrium" value at large droplet sizes provides a quantitative measure for interfacial tension. Next to the reference case of pure PE/PP, the PPH/ICP with unmodified and interpolated TREF input is shown. The results for PPH/ICP system are being shown for the cases with and without intrachain compositional fluctuations.

For the unmodified TREF input, the interfacial tension is given by 1.2×10^{-3} J/m^2, whereas the corresponding value for the interpolated case is 0.8×10^{-3} J/m^2. The pure PE/PP blend exhibits a value of 1.7×10^{-3} J/m^2. As a result of the much less complex composition, the size dependence of the interfacial tension is markedly weaker for the pure blend.

Clearly, the division of the amorphous part in three components, decreasing the composition gap between the amorphous composition as given by the unmodified TREF data and its neighboring layers, significantly reduces interfacial tension. Comparison of the values of a PPH/ICP system to a pure PP/PE system reveals that a more gradual ethylene gradient leads to lower interfacial tensions. It is also seen that introducing representative intrachain fluctuations does not lead to a significant decrease of the interfacial tension. Somewhat unexpectedly, the effect of intrachain composition fluctuation leads to a slight increase in interfacial tension for the interpolated case. The increase in tension can probably be attributed to the fact that, due to the randomness in chain composition, some chains have a higher ethylene content than their averaged counterparts. This elevated ethylene content for some components can lead to a higher tension.

How well do the simulations predict actual morphology?

Although the simulations described so far provide a comprehensive picture of the morphology development under static conditions, the question remains in how far a clue is provided regarding morphology in practical conditions, as this obviously determines the final properties of the material. This question is certainly not trivial, because in practice, morphology is formed during processing.

On one hand, the incompatibility of both phases will provide a thermodynamic driving force toward coagulation of the rubber phase, and on the other hand, the shear forces will result in breakdown of droplets. A kind of dynamic equilibrium results between these two processes, which is frozen in during cooling after processing. For this reason, the actual morphology is not expected to show nicely separated rubber particles with a well-defined size distribution, but rather a mixture of various phases of the dynamic process.

There are some experimental approaches which prove to be helpful to qualitatively clarify the droplet morphology after processing. In this way it can

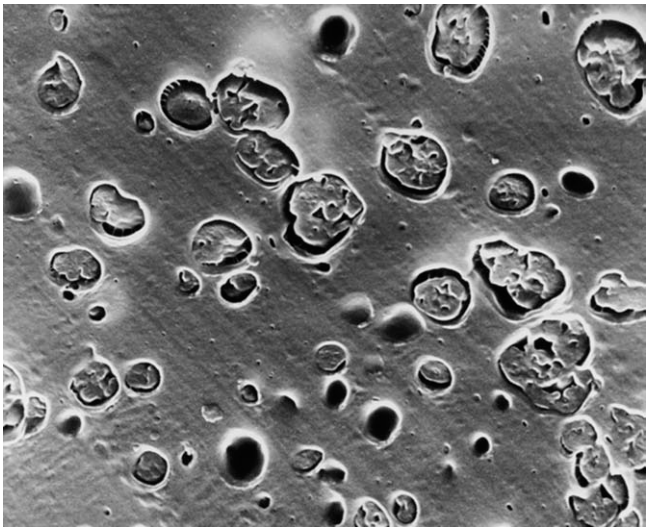

Figure 11 SEM image of a typical ICP morphology obtained by secondary electron imaging after hexane extraction at 60°C. Darker regions indicate cavities where material was extracted. This roughly corresponds to amorphous copolymer with ethylene content up to 80–85%.

be determined to what extent equilibrium simulations are of value during processing conditions. The basis for these approaches is formed by the composition distribution. As polymer chains with very high ethylene contents potentially crystallize and the parts of the composition distribution with low ethylene content are completely amorphous, a stratified morphology should result in a kind of "crystallinity gradient." Experimental techniques that would be able to probe such gradients are for instance transmission electron microscopy (TEM), atomic force microscopy (AFM), scanning electron microscopy (SEM), and possibly microthermal analysis.[37]

Support for the existence of a crystallinity gradient is provided by SEM images. In SEM, a polymer surface is extracted with a solvent that completely dissolves amorphous material. Therefore, this treatment should result in an image in which the core of the rubber particle is still visible (the crystallizing components in the distribution), whereas at the interface between rubber and matrix essentially all material is dissolved. This is actually observed in practice as shown in Figure 11.

Moreover, recent development in AFM techniques provides the opportunity to zoom in on the details of rubber morphology. Quantitative nanomechanical mapping (QNM) is an AFM-based technique providing the modulus differences present in a flat cross section of a sample (e.g., see Ref. 38). Figure 12 shows an example of such an evaluation for an ICP.

Again it is clearly observed that the highest modulus parts are in the center of the particle. When interpreting this image it must be kept in mind that the modulus gradient is not expected to be gradual. Although PE crystallizes very fast, even small amount of comonomer have a detrimental effect on crystallizability, with a corresponding effect on the modulus. Therefore, the highest ethylene-containing components will show a relatively high modulus (typically in the GPa range), whereas the modulus will drop fast to rubber-like values in the MPa range below $\sim$ 80 to 85 wt % of ethylene. This latter threshold constitutes a reasonable assumption that extractability by hexane at 60°C coincides with the onset of regular semicrystallinity. Although a quantitative evaluation of the modulus data within the amorphous regions is not feasible (it would require a varying modulus response with varying ethylene content, which does not exist), an estimate in the order of 35 wt % crystallizing material—based on TREF data—seems reasonable. The results of both methods demonstrate that indeed the thermodynamic drive toward stratified droplet morphology is evidently present.

CONCLUSIONS

In this study, the equilibrium morphology of a PP ICP system consisting of an EPR droplet surrounded by a PP matrix was investigated in the molten state. Computer simulations were carried out using a software package, CULGI, based on numerical SCF calculations.

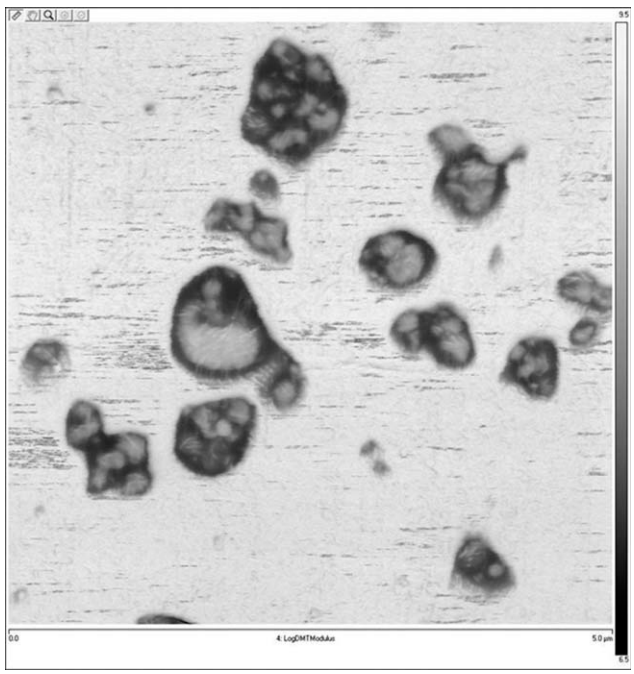

Figure 12 AFM-QNM picture of a typical ICP. The right side of the image provides a logarithmic scale of the local modulus ranging from semicrystalline (GPa range in white) to rubbery (MPa range in black) domain.

The analytical data for the ICP, i.e., MM, MMD, and CCD, were determined using preparative TREF followed by SEC-DV and ^{13}C-NMR and were translated into CULGI parameters, i.e., number of beads and number of components, each one being characterized by its own ethylene content.

The influence of a major drawback of TREF, i.e., the inability to quantify the CCD of the amorphous part of the material, was investigated by introducing an interpolated case of an artificial distribution of the amorphous material of three components. It is shown that typical ICPs with a broad CCD form a stratified equilibrium morphology.

The most critical parameter for the location of a component within a droplet is shown to be the ethylene content. A component exhibiting high ethylene content is usually found in the vicinity of the droplet core, whereas a component with low ethylene content is mainly found close to the PP matrix. The low molecular weight promotes leakage to neighboring compositions; however, this is a secondary effect when compared with the influence of ethylene content. Furthermore, a comparison of unmodified with interpolated TREF input did not reveal dramatic differences between the equilibrium morphologies.

However, inevitably ICPs go through a processing step, in which high shear is involved. Although thermodynamic forces will promote aggregation of rubber droplets, shear will have a reverse effect. Obviously, during processing, thermodynamic equilibrium does not reflect real morphology. In contrary, a sort of dynamic equilibrium, governed by the balance of forces promoting aggregation and dispersion, will be more realistic. In this balance, interfacial tension provides an important parameter.

Therefore, a procedure recently developed by us has been applied to estimate the difference in interfacial tension between both cases simulated. It may be concluded that smooth gradients in ethylene content lead to lower interfacial tension as observed by both the interpolated extra breakdown of the 37% ethylene fraction and comparison between pure PE/PP and HPP/ICP. It has also been found that including intrachain compositional fluctuations do not lead to significant reductions in interfacial tension. In compositionally disperse ICP systems, material exchange from droplet to droplet (which can be expected to be an important process in reaching a "dynamic equilibrium" under specified process conditions) has not been taken into account. Therefore, this being an important step toward a complete understanding of morphology formation in complex blends, we are presently conducting simulations taking into account the effect of shear. However, notwithstanding the fact that this system is processed far from equilibrium, still quite a few essential features of the real morphology are borne out by our equilibrium simulations. This is explicitly shown by comparing the simulation results of the droplet morphology with TEM, SEM, and AFM-QNM images. In particular, the stratified structure where the droplet shows increasing ethylene content toward the droplet core is predicted by the present simulation and is revealed in the microscopical observations.

The authors thank Prof. J. G. E. M. Fraaije and Dr. J. van Male (CULGI B.V.) for their support. They are indebted to Dr. R. A. C. Deblieck (DSM Resolve) for fruitful discussions, critical reading of the manuscript, and providing EM images and to Dr. R. Kleppinger (DSM Resolve) for the AFM-QNM results.

References

1. Polypropylene Handbook, 2nd ed.; Pasquini, N., Ed.; Carl Hanser Verlag: Munich, 2005; Chapters 1, 9, and 10.
2. Polypropylene Handbook, 2nd ed.; Pasquini, N., Ed.; Carl Hanser Verlag: Munich, 2005; Chapters 5, 9, and 10.
3. Polypropylene Handbook, 2nd ed.; Pasquini, N., Ed.; Carl Hanser Verlag: Munich, 2005; Chapters 1, 2, and 6.
4. Debling, J. A.; Ray, W. H. J Appl Polym Sci 2001, 81, 3085.
5. Kakugo, M.; Sadatoshi, H.; Yokoyama, M.; Kojima, K. Macromolecules 1989, 22, 551.
6. Kakugo, M.; Sadatoshi, H.; Sakai, J.; Yokoyama, M. Macromolecules 1989, 22, 3172.
7. Kamdar, A. R.; Hu, Y. S.; Ansems, P.; Chum, S. P.; Hiltner, A.; Baer, E. Macromolecules 2006, 39, 1496.
8. Kissin, Y. V.; Ohnishi, R.; Konakazawa, T. Macromol Chem Phys 2004, 205, 284.
9. Kissin, Y. V.; Rishina, L. A. Polym Sci Ser A 2008, 50, 1101.
10. Feng, Y.; Hay, J. N. Polymer 1998, 39, 6723.
11. Cai, H.; Luo, X.; Ma, D.; Wang, J.; Tan, H. J Appl Polym Sci 1999, 71, 93.
12. Cai, H.; Luo, X.; Ma, D.; Wang, J.; Tan, H. J Appl Polym Sci 1999, 71, 103.
13. Kissin, Y. V.; Fruitwala, H. A. J Appl Polym Sci 2007, 106, 3872.
14. Kissin, Y. V.; Mirabella, F. M.; Meverden, C. C. J Polym Sci Part A: Polym Chem 2005, 43, 4351.
15. Fan, Z. Q.; Zhang, Y. Q.; Xu, J. T.; Wang, H. T.; Feng, L. X. Polymer 2001, 42, 5559.
16. Fu, Z. S.; Fan, Z. Q.; Zhang, Y. Q.; Feng, L. X. Eur Polym J 2003, 39, 795.
17. Zhu, H.; Monrabal, B.; Han, C. C.; Wang, D. Macromolecules 2008, 41, 826.
18. Tan, H.; Li, L.; Chen, Z.; Song, Y.; Zheng, Q. Polymer 2005, 46, 3522.
19. Grein, C.; Bernreitner, K.; Hauer, A.; Gahleitner, M.; Neißl, W. J Appl Polym Sci 2003, 87, 1702.
20. Polypropylene Handbook, 2nd ed.; Pasquini, N., Ed.; Carl Hanser Verlag: Munich, 2005; Chapter 3..
21. Utracki, L. A.; Dumoulin, M. M. In Polypropylene: Structure, Blends and Composites; Karger-Kocsis, J., Ed.; Chapman and Hall: London, 1995; Vol.2, Chapter 3.
22. Doshev, P.; Lohse, S. H.; Krumova, M.; Heuvelsland, A.; Michler, G.; Radusch, H. J. J Appl Polym Sci 2006, 101, 2825.
23. Polypropylene Handbook, 2nd ed.; Pasquini, N., Ed.; Carl Hanser Verlag: Munich, 2005; Chapters 3 and 7.
24. Fortelný, I.; Michálková, D.; Koplíková, J.; Navrátilová, E.; Kovář, J. Angew Makromol Chem 1990, 179, 185.
25. Flory, P. J. Principles of Polymer Chemistry; Cornell University Press: Ithaca, New York, 1953.

26. Fraaije, J. G. E. M. J Chem Phys 1993, 99, 9202.
27. Fredrickson, G. H.; Ganesan, V.; Drolet, F. Macromolecules 2002, 35, 16.
28. Helfand, E. J Chem Phys 1975, 62, 999.
29. Fraaije, J. G. E. M.; Remerie, K.; Groenewold, J. Macromol Theory Simul 2011, 20, 133.
30. Lohse, D. J.; Greassly, W. W. In Polymer Blends; Paul, D. R.; Bucknall, C. B., Eds.; Wiley-Interscience: New York, 2000; Vol.1, p 219.
31. Scott, R. L. J Polym Sci 1952, 9, 423.
32. Ten Brinke, G.; Karasz, F. E.; MacKnight, W. J. Macromolecules 1983, 16, 1827.
33. Groenewold, J.; Remerie, K. Macromol Theory Simul 2010, 19, 370.
34. Donley, J. P.; Fredrickson, G. H. J Polym Sci Part B: Polym Phys 1992, 30, 1527.
35. Helfand, E.; Tagami, Y. J Polym Sci Part B: Polym Lett 1971, 9, 741.
36. Fetters, L. J.; Lohse, D. J.; Colby, R. H. In Physical Properties of Polymers, 2nd ed.; Mark, J. H., Ed.; 2007; Chapter 25, Springer, New York, p 447.
37. Reading, M.; Price, D. M.; Grandy, D. B.; Smith, R. M.; Bozec, L.; Conroy, M.; Hammiche, A.; Pollock, H. M. Makromol Symp 2001, 167, 45.
38. Schön, P.; Bagdi, K.; Molnár, K.; Markus, P.; Pukánszky, B.; Vancso, G. J. Eur Polym J 2011, 47, 692.